Nanoscale plasmonic phenomena in CVD-grown MoS_2 monolayer revealed by ultra-broadband synchrotron radiation based nano-FTIR spectroscopy and near-field microscopy

Piotr Patoka,[1,*] Georg Ulrich,[1] Ariana E. Nguyen,[2] Ludwig Bartels,[2] Peter A. Dowben,[3] Volodymyr Turkowski,[4] Talat S. Rahman,[4] Peter Hermann,[5] Bernd Kästner,[5] Arne Hoehl,[5] Gerhard Ulm,[5] and Eckart Rühl,[1,*]

[1]*Physikalische Chemie, Institut für Chemie und Biochemie, Freie Universität Berlin, Takustr. 3, 14195 Berlin, Germany*

[2]*Department of Chemistry, University of California Riverside, 0124 Pierce Hall, Riverside, 92521 California, USA*

[3]*Department of Physics and Astronomy, University of Nebraska – Lincoln, T. Jorgensen Hall, Lincoln, 68588-0299 Nebraska, USA*

[4]*Department of Physics, University of Central Florida, 4000 Central Florida Blvd., Orlando, 32816-2385 Florida, USA*

[5]*Physikalisch-Technische Bundesanstalt, Abbestraße 2-12, 10587 Berlin, Germany*

[*]*ruehl@zedat.fu-berlin.de*

Abstract: Nanoscale plasmonic phenomena observed in single and bi-layers of molybdenum disulfide (MoS_2) on silicon dioxide (SiO_2) are reported. A scattering type scanning near-field optical microscope (s-SNOM) with a broadband synchrotron radiation (SR) infrared source was used. We also present complementary optical mapping using tunable CO_2-laser radiation. Specifically, there is a correlation of the topography of well-defined MoS_2 islands grown by chemical vapor deposition, as determined by atomic force microscopy, with the infrared (IR) signature of MoS_2. The influence of MoS_2 islands on the SiO_2 phonon resonance is discussed. The results reveal the plasmonic character of the MoS_2 structures and their interaction with the SiO_2 phonons leading to an enhancement of the hybridized surface plasmon-phonon mode. A theoretical analysis shows that, in the case of monolayer islands, the coupling of the MoS_2 optical plasmon mode to the SiO_2 surface phonons does not affect the infrared spectrum significantly. For two-layer MoS_2, the coupling of the extra inter-plane acoustic plasmon mode with the SiO_2 surface transverse phonon leads to a remarkable increase of the surface phonon peak at 794 cm^{-1}. This is in agreement with the experimental data. These results show the capability of the s-SNOM technique to study local multiple excitations in complex non-homogeneous structures.

OCIS codes: (120.0120) Instrumentation, measurement, and metrology; (180.4243) Near-field microscopy; (240.0310) Thin films; (300.6340) Spectroscopy, infrared; (310.6188) Spectral properties.

References and links

1. J. A. Wilson and A. D. Yoffe, "The transition metal dichalcogenides discussion and interpretation of the observed optical, electrical and structural properties," Adv. Phys. **18**(73), 193–335 (1969).
2. K. F. Mak, C. Lee, J. Hone, J. Shan, and T. F. Heinz, "Atomically thin MoS_2: a new direct-gap semiconductor," Phys. Rev. Lett. **105**(13), 136805 (2010).
3. J. Mann, Q. Ma, P. M. Odenthal, M. Isarraraz, D. Le, E. Preciado, D. Barroso, K. Yamaguchi, G. von Son Palacio, A. Nguyen, T. Tran, M. Wurch, A. Nguyen, V. Klee, S. Bobek, D. Sun, T. F. Heinz, T. S. Rahman, R.

#252198 Received 19 Oct 2015; revised 17 Dec 2015; accepted 19 Dec 2015; published 13 Jan 2016

Corrected: 22 February 2016

Kawakami, and L. Bartels, "2-dimensional transition metal dichalcogenides with tunable direct band gaps: $MoS_{2(1-x)}$ Se_2x monolayers," Adv. Mater. **26**(9), 1399–1404 (2014).
4. S. Y. Zhou, G.-H. Gweon, A. V. Fedorov, P. N. First, W. A. de Heer, D.-H. Lee, F. Guinea, A. H. Castro Neto, and A. Lanzara, "Substrate-induced bandgap opening in epitaxial graphene," Nat. Mater. **6**(10), 770–775 (2007).
5. R. Balog, B. Jørgensen, L. Nilsson, M. Andersen, E. Rienks, M. Bianchi, M. Fanetti, E. Laegsgaard, A. Baraldi, S. Lizzit, Z. Sljivancanin, F. Besenbacher, B. Hammer, T. G. Pedersen, P. Hofmann, and L. Hornekaer, "Bandgap opening in graphene induced by patterned hydrogen adsorption," Nat. Mater. **9**(4), 315–319 (2010).
6. K. Nakada, M. Fujita, G. Dresselhaus, and M. S. Dresselhaus, "Edge state in graphene ribbons: Nanometer size effect and edge shape dependence," Phys. Rev. B Condens. Matter **54**(24), 17954–17961 (1996).
7. Y.-W. Son, M. L. Cohen, and S. G. Louie, "Energy gaps in graphene nanoribbons," Phys. Rev. Lett. **97**(21), 216803 (2006).
8. M. Y. Han, B. Özyilmaz, Y. Zhang, and P. Kim, "Energy band-gap engineering of graphene nanoribbons," Phys. Rev. Lett. **98**(20), 206805 (2007).
9. M.-W. Lin, C. Ling, Y. Zhang, H. J. Yoon, M.-M. C. Cheng, L. A. Agapito, N. Kioussis, N. Widjaja, and Z. Zhou, "Room-temperature high on/off ratio in suspended graphene nanoribbon field-effect transistors," Nanotechnology **22**(26), 265201 (2011).
10. L. Ci, L. Song, C. Jin, D. Jariwala, D. Wu, Y. Li, A. Srivastava, Z. F. Wang, K. Storr, L. Balicas, F. Liu, and P. M. Ajayan, "Atomic layers of hybridized boron nitride and graphene domains," Nat. Mater. **9**(5), 430–435 (2010).
11. A. H. Castro Neto, F. Guinea, N. M. R. Peres, K. S. Novoselov, and A. K. Geim, "The electronic properties of graphene," Rev. Mod. Phys. **81**(1), 109–162 (2009).
12. P. Avouris, "Graphene: electronic and photonic properties and devices," Nano Lett. **10**(11), 4285–4294 (2010).
13. S. Das Sarma, S. Adam, E. H. Hwang, and E. Rossi, "Electronic transport in two-dimensional graphene," Rev. Mod. Phys. **83**(2), 407–470 (2011).
14. Q. Yue, J. Kang, Z. Shao, X. Zhang, S. Chang, G. Wang, S. Qin, and J. Li, "Mechanical and electronic properties of monolayer MoS_2 under elastic strain," Phys. Lett. A **376**(12-13), 1166–1170 (2012).
15. A. Molina-Sánchez, D. Sangalli, K. Hummer, A. Marini, and L. Wirtz, "Effect of spin-orbit interaction on the optical spectra of single-layer, double-layer, and bulk MoS_2," Phys. Rev. B **88**(4), 045412 (2013).
16. A. N. Grigorenko, M. Polini, and K. S. Novoselov, "Graphene plasmonics," Nat. Photonics **6**(11), 749–758 (2012).
17. T. Low and P. Avouris, "Graphene plasmonics for terahertz to mid-infrared applications," ACS Nano **8**(2), 1086–1101 (2014).
18. T. Stauber, "Plasmonics in Dirac systems: from graphene to topological insulators," J. Phys. Condens. Matter **26**(12), 123201 (2014).
19. M. Polini, R. Asgari, G. Borghi, Y. Barlas, T. Pereg-Barnea, and A. H. MacDonald, "Plasmons and the spectral function of graphene," Phys. Rev. B **77**(8), 081411 (2008).
20. A. Scholz, T. Stauber, and J. Schliemann, "Plasmons and screening in a monolayer of MoS_2," Phys. Rev. B **88**(3), 035135 (2013).
21. P. Alonso-González, A. Y. Nikitin, F. Golmar, A. Centeno, A. Pesquera, S. Vélez, J. Chen, G. Navickaite, F. Koppens, A. Zurutuza, F. Casanova, L. E. Hueso, and R. Hillenbrand, "Controlling graphene plasmons with resonant metal antennas and spatial conductivity patterns," Science **344**(6190), 1369–1373 (2014).
22. K. M. Goodfellow, R. Beams, C. Chakraborty, L. Novotny, and A. N. Vamivakas, "Integrated nanophotonics based on nanowire plasmons and atomically thin material," Optica **1**(3), 149–152 (2014).
23. S. Butun, S. Tongay, and K. Aydin, "Enhanced light emission from large-area monolayer MoS_2 using plasmonic nanodisc arrays," Nano Lett. **15**(4), 2700–2704 (2015).
24. Ž. Bonačić Lošić, "Coupling of plasmon and dipolar modes in a monolayer of MoS_2," Mod. Phys. Lett. B **28**(12), 1450099 (2014).
25. G. Plechinger, J. Mann, E. Preciado, D. Barroso, A. Nguyen, J. Eroms, C. Schüller, L. Bartels, and T. Korn, "A direct comparison of CVD-grown and exfoliated MoS_2 using optical spectroscopy," Semicond. Sci. Technol. **29**(6), 064008 (2014).
26. A. M. van der Zande, P. Y. Huang, D. A. Chenet, T. C. Berkelbach, Y. You, G.-H. Lee, T. F. Heinz, D. R. Reichman, D. A. Muller, and J. C. Hone, "Grains and grain boundaries in highly crystalline monolayer molybdenum disulphide," Nat. Mater. **12**(6), 554–561 (2013).
27. C. Lee, H. Yan, L. E. Brus, T. F. Heinz, J. Hone, and S. Ryu, "Anomalous lattice vibrations of single- and few-layer MoS_2," ACS Nano **4**(5), 2695–2700 (2010).
28. H. Li, Q. Zhang, C. Yap, B. Tay, T. Edwin, A. Olivier, and D. Baillargeat, "From bulk to monolayer MoS_2: evolution of Raman scattering," Adv. Funct. Mater. **22**(7), 1385–1390 (2012).
29. F. Bonaccorso, P.-H. Tan, and A. C. Ferrari, "Multiwall nanotubes, multilayers, and hybrid nanostructures: new frontiers for technology and Raman spectroscopy," ACS Nano **7**(3), 1838–1844 (2013).
30. X. Yin, Z. Ye, D. A. Chenet, Y. Ye, K. O'Brien, J. C. Hone, and X. Zhang, "Edge Nonlinear Optics on a MoS_2 Atomic Monolayer," Science **344**(6183), 488–490 (2014).
31. N. Kumar, A. Rae, and D. Roy, "Accurate measurement of enhancement factor in tip-enhanced Raman spectroscopy through elimination of far-field artefacts," Appl. Phys. Lett. **104**(12), 123106 (2014).
32. L. M. Malard, T. V. Alencar, A. P. M. Barboza, K. F. Mak, and A. M. de Paula, "Observation of intense second harmonic generation from MoS_2 atomic crystals," Phys. Rev. B **87**(20), 201401 (2013).

#252198 Received 19 Oct 2015; revised 17 Dec 2015; accepted 19 Dec 2015; published 13 Jan 2016

33. N. Kumar, S. Najmaei, Q. Cui, F. Ceballos, P. M. Ajayan, J. Lou, and H. Zhao, "Second harmonic microscopy of monolayer MoS_2," Phys. Rev. B **87**(16), 161403 (2013).
34. Y. Lin, X. Ling, L. Yu, S. Huang, A. L. Hsu, Y.-H. Lee, J. Kong, M. S. Dresselhaus, and T. Palacios, "Dielectric screening of excitons and trions in single-layer MoS_2," Nano Lett. **14**(10), 5569–5576 (2014).
35. K. Andersen, K. W. Jacobsen, and K. S. Thygesen, "Plasmons on the edge of MoS_2 nanostructures," Phys. Rev. B **90**(16), 161410 (2014).
36. Z. Fei, G. O. Andreev, W. Bao, L. M. Zhang, A. S McLeod, C. Wang, M. K. Stewart, Z. Zhao, G. Dominguez, M. Thiemens, M. M. Fogler, M. J. Tauber, A. H. Castro-Neto, C. N. Lau, F. Keilmann, and D. N. Basov, "Infrared nanoscopy of Dirac plasmons at the graphene-SiO□ interface," Nano Lett. **11**(11), 4701–4705 (2011).
37. Z. Fei, A. S. Rodin, G. O. Andreev, W. Bao, A. S. McLeod, M. Wagner, L. M. Zhang, Z. Zhao, M. Thiemens, G. Dominguez, M. M. Fogler, A. H. Castro Neto, C. N. Lau, F. Keilmann, and D. N. Basov, "Gate-tuning of graphene plasmons revealed by infrared nano-imaging," Nature **487**(7405), 82–85 (2012).
38. J. Chen, M. Badioli, P. Alonso-González, S. Thongrattanasiri, F. Huth, J. Osmond, M. Spasenović, A. Centeno, A. Pesquera, P. Godignon, A. Z. Elorza, N. Camara, F. J. García de Abajo, R. Hillenbrand, and F. H. L. Koppens, "Optical nano-imaging of gate-tunable graphene plasmons," Nature **487**(7405), 77–81 (2012).
39. M. Wagner, Z. Fei, A. S. McLeod, A. S. Rodin, W. Bao, E. G. Iwinski, Z. Zhao, M. Goldflam, M. Liu, G. Dominguez, M. Thiemens, M. M. Fogler, A. H. Castro Neto, C. N. Lau, S. Amarie, F. Keilmann, and D. N. Basov, "Ultrafast and nanoscale plasmonic phenomena in exfoliated graphene revealed by infrared pump-probe nanoscopy," Nano Lett. **14**(2), 894–900 (2014).
40. S. Kawata and Y. Inouye, "Scanning probe optical microscopy using a metallic probe tip," Ultramicroscopy **57**(2-3), 313–317 (1995).
41. F. Zenhausern, Y. Martin, and H. K. Wickramasinghe, "Scanning interferometric apertureless microscopy: optical imaging at 10 angstrom resolution," Science **269**(5227), 1083–1085 (1995).
42. R. Bachelot, P. Gleyzes, and A. C. Boccara, "Near-field optical microscope based on local perturbation of a diffraction spot," Opt. Lett. **20**(18), 1924–1926 (1995).
43. B. Knoll and F. Keilmann, "Near-field probing of vibrational absorption for chemical microscopy," Nature **399**(6732), 134–137 (1999).
44. F. Huth, A. Govyadinov, S. Amarie, W. Nuansing, F. Keilmann, and R. Hillenbrand, "Nano-FTIR absorption spectroscopy of molecular fingerprints at 20 nm spatial resolution," Nano Lett. **12**(8), 3973–3978 (2012).
45. Y. Ikemoto, T. Moriwaki, T. Kinoshita, M. Ishikawa, S. Nakashima, and H. Okamura, "Near-field spectroscopy with infrared synchrotron radiation source," J. Surf. Sci. Nanotech. **9**, 63–66 (2011).
46. P. Hermann, A. Hoehl, P. Patoka, F. Huth, E. Rühl, and G. Ulm, "Near-field imaging and nano-Fourier-transform infrared spectroscopy using broadband synchrotron radiation," Opt. Express **21**(3), 2913–2919 (2013).
47. P. Hermann, A. Hoehl, G. Ulrich, C. Fleischmann, A. Hermelink, B. Kästner, P. Patoka, A. Hornemann, B. Beckhoff, E. Rühl, and G. Ulm, "Characterization of semiconductor materials using synchrotron radiation-based near-field infrared microscopy and nano-FTIR spectroscopy," Opt. Express **22**(15), 17948–17958 (2014).
48. H. A. Bechtel, E. A. Muller, R. L. Olmon, M. C. Martin, and M. B. Raschke, "Ultrabroadband infrared nanospectroscopic imaging," Proc. Natl. Acad. Sci. U.S.A. **111**(20), 7191–7196 (2014).
49. F. Peragut, J.-B. Brubach, P. Roy, and Y. De Wilde, "Infrared near-field imaging and spectroscopy based on thermal or synchrotron radiation," Appl. Phys. Lett. **104**(25), 251118 (2014).
50. J. Feikes, M. von Hartrott, M. Ries, P. Schmid, G. Wüstefeld, A. Hoehl, R. Klein, R. Müller, and G. Ulm, "Metrology Light Source: The first electron storage ring optimized for generating coherent THz radiation," Phys. Rev. ST Accel. Beams **14**(3), 030705 (2011).
51. N. Ocelic, A. Huber, and R. Hillenbrand, "Pseudoheterodyne detection for background-free Near-field spectroscopy," Appl. Phys. Lett. **89**(10), 101124 (2006).
52. J. Mann, D. Sun, Q. Ma, J.-R. Chen, E. Preciado, T. Ohta, B. Diaconescu, K. Yamaguchi, T. Tran, M. Wurch, K. Magnone, T. F. Heinz, G. L. Kellogg, R. Kawakami, and L. Bartels, "Facile growth of monolayer MoS_2 film areas on SiO_2," Eur. Phys. J. B **86**(5), 226 (2013).
53. R. F. Frindt, "Single crystals of MoS_2 several molecular layers thick," J. Appl. Phys. **37**(4), 1928–1929 (1966).
54. P. Nemes-Incze, Z. Osváth, K. Kamarás, and L. P. Biró, "Anomalies in thickness measurements of graphene and few layer graphite crystals by tapping mode atomic force microscopy," Carbon **46**(11), 1435–1442 (2008).
55. A. A. Govyadinov, S. Mastel, F. Golmar, A. Chuvilin, P. S. Carney, and R. Hillenbrand, "Recovery of permittivity and depth from near-field data as a step toward infrared nanotomography," ACS Nano **8**(7), 6911–6921 (2014).
56. F. Maugé, J. Lamotte, N. S. Nesterenko, O. Manoilova, and A. A. Tsyganenko, "FT-IR study of surface properties of unsupported MoS_2," Catal. Today **70**(1-3), 271–284 (2001).
57. A. Molina-Sánchez and L. Wirtz, "Phonons in single-layer and few-layer MoS_2 and WS_2," Phys. Rev. B **84**(15), 155413 (2011).
58. M. Ishikawa, M. Katsura, S. Nakashima, Y. Ikemoto, and H. Okamura, "Broadband near-field mid-infrared spectroscopy and application to phonon resonances in quartz," Opt. Express **20**(10), 11064–11072 (2012).
59. A. J. Huber, J. Wittborn, and R. Hillenbrand, "Infrared spectroscopic near-field mapping of single nanotransistors," Nanotechnology **21**(23), 235702 (2010).
60. S. Amarie and F. Keilmann, "Broadband-infrared assessment of phonon resonance in scattering-type near-field microscopy," Phys. Rev. B **83**(4), 045404 (2011).

#252198 Received 19 Oct 2015; revised 17 Dec 2015; accepted 19 Dec 2015; published 13 Jan 2016

61. A. S. McLeod, P. Kelly, M. D. Goldflam, Z. Gainsforth, A. J. Westphal, G. Dominguez, M. H. Thiemens, M. M. Fogler, and D. N. Basov, "Model for quantitative tip-enhcanced spectroscopy and the extraction of nanoscale-resolved optical constants," Phys. Rev. B **90**(8), 085136 (2014).
62. W. G. Spitzer and D. A. Kleinman, "Infrared lattice bands of quartz," Phys. Rev. **121**(5), 1324–1335 (1961).
63. E. H. Hwang, R. Sensarma, and S. Das Sarma, "Plasmon-phonon coupling in graphene," Phys. Rev. B **82**(19), 195406 (2010).
64. R. Hillenbrand and F. Keilmann, "Complex optical constants on a subwavelength scale," Phys. Rev. Lett. **85**(14), 3029–3032 (2000).
65. T. Stauber and G. Gómez-Santos, "Plasmons and near-field amplification in double-layer graphene," Phys. Rev. B **85**(7), 075410 (2012).
66. R. E. V. Profumo, R. Asgari, M. Polini, and A. H. MacDonald, "Double-layer graphene and topological insulator thin-film plasmons," Phys. Rev. B **85**(8), 085443 (2012).
67. N. Kumar, Q. Cui, F. Ceballos, D. He, Y. Wang, and H. Zhao, "Exciton diffusion in monolayer and bulk $MoSe_2$," Nanoscale **6**(9), 4915–4919 (2014).
68. A. C. Ferrari and D. M. Basko, "Raman spectroscopy as a versatile tool for studying the properties of graphene," Nat. Nanotechnol. **8**(4), 235–246 (2013).

1. Introduction

Among the 2D electronic materials that have received increased attention recently are the transition metal dichalcogenides. They consist of hexagonally structured layers of metal atoms, typically Mo, or W-embedded between two layers of chalcogenes (typically S, Se, or Te) [1], although the overall point group symmetry is C_{3v}. Depending on the combination of the metal and the chalcogen, different material properties are obtained. In this work we focus on MoS_2. In contrast to graphene, MoS_2 is another intensely studied 2D electronic material, but has a direct band gap (E_g = 1.87 eV) in the monolayer limit [2, 3] and therefore does not require influence of the substrate [4], substrate hydrogen passivation [5], or dimensional reduction to break metallicity [6–9]. Likewise doping with nitrogen or boron [10] is not possible for MoS_2. There is extensive literature for both MoS_2 and graphene describing their electronic [1, 2, 11–15] as well as plasmonic properties [16–20], partially because of their potential in plasmonic circuitry [21–23].

There are important, characteristic differences between MoS_2 and graphene: for instance, in graphene the low-energy collective oscillations originate from intraband electron resonances [20], whereas in single layer MoS_2 (1L-MoS_2) there are not only a low-energy oscillations [18, 20] but also a coupled system with an interband dipolar collective mode, which lowers the plasmon dispersion [24]. Specific emphasis was put on the electronic and optical properties of 1L-MoS_2, as probed by photoluminescence (PL) spectroscopy [2, 3, 25, 26], Raman spectroscopy [27–29], and second harmonic generation [30–33]. These methods make use of primary excitation in the optical regime. The use of photons with energies exceeding the 1L-MoS_2 direct band gap leads to exciton modes that are present in photoluminescence (PL) measurements [34], as well as strongly damped plasmons, in which energy losses are connected to the interband transition processes. The latter ones reduce the transition energy and the lifetime of the plasmons [35]. Direct excitation of the intraband plasmons in such systems requires, however, infrared (IR) radiation. Since the wavevector of the plasmons in extended monolayer graphene or 1L-MoS_2 is much larger than the wavevector of freely propagating photons of the same energy, one needs to find a way to overcome this mismatch for the successful excitation of plasmon polaritons.

Recent experiments by Fourier-transform infrared (FTIR) nanoscopy and nanoimaging on exfoliated graphene demonstrated that confining IR radiation to a nanosized scattering object results in an increased coupling to the in-plane momentum component and thus enables the optical excitation of plasmons [36–39]. These experiments used the near-field based technique namely scattering-type scanning near-field optical microscopy (s-SNOM) [40–43]. This method has gained broad interest because it not only enables imaging with a spatial resolution below 20 nm [44] but in combination with a broadband IR radiation source i.e., difference frequency generation sources [44] or ultra-broadband synchrotron radiation [45–49], it allows for probing the spectroscopic response of nanoscale objects as well as thin films.

#252198 Received 19 Oct 2015; revised 17 Dec 2015; accepted 19 Dec 2015; published 13 Jan 2016

Here, we present high sensitivity imaging and nano-FTIR spectroscopy on 1L-MoS_2 samples using the electron storage ring Metrology Light Source (MLS) [46, 47, 50] in the mid-IR regime. We demonstrate that plasmonic enhancement of the SiO_2 phonon due to coupling with the plasmon from a 2D material does not require the presence of an adlayer that exhibits a "Dirac cone plasmon", as surmised from previous experiments on exfoliated graphene [39]. At fixed carrier concentration, the optical plasmon frequency in 1L-MoS_2 is significantly lower as compared to the graphene plasmon frequency. Therefore, in order to observe the effect of the exciton-plasmon coupling in 1L-MoS_2 on SiO_2, one needs an order of magnitude higher carrier concentrations in MoS_2 compared to graphene. However, one can already observe an enhancement of the SiO_2 phonons by the MoS_2 plasmon in the case of the double layer (2L-MoS_2), i.e. at rather low charge carrier concentration levels. Specifically, as is demonstrated below, we observe in the case of 2L-MoS_2 an additional inter-layer (acoustic) plasmon mode which is coupled to the corresponding SiO_2 transverse phonon mode. This leads to a significant increase in intensity in the s-SNOM spectrum, as shown here.

2. Experimental part

The experimental setup has been described previously [46, 47]. It consists of a commercial s-SNOM system (NeaSNOM, Neaspec GmbH, Germany), which combines an atomic force microscope (AFM) operating in tapping mode with a typical oscillation amplitude of about 50 nm and an asymmetric Michelson interferometer. Au-coated silicon AFM cantilevers with a metal layer thickness of about 20 nm and resonance frequencies in the range from 75 to 265 kHz were used for the experiments described below. The average tip diameter of near-field probes did not exceed 50 nm. As an IR radiation source we either used a continuous wave, grating-tuned CO_2 gas laser (PL5, Edinburgh Instruments, UK) working in sealed-off mode or the IR radiation from the MLS storage ring (Berlin, Germany). The former source is characterized by high intensity and frequency stability at discrete transition lines enhancing suitability for nano-imaging experiments. The latter source is predominantly designed as an ultra-broadband source for spectroscopy by delivering high brilliance radiation in the IR and THz regimes.

In our experiments the emitted synchrotron radiation (SR) was directed to the experimental setup from the storage ring by using several parabolic and planar mirrors. At the end of the beamline a diamond window is mounted. From there the radiation penetrates ambient conditions under which the s-SNOM experiments were carried out. At this point the IR beam has a rhomboidal shape of approximately 10 mm x 25 mm in vertical and horizontal directions, respectively. The integrated power was typically about 2 mW in the wavelength range from 1 μm to 20 μm at a ring current of 100 mA. The radiation is then guided through a periscope-like mirror configuration [P in Fig. 1], in order to convert the initial horizontal polarization of the SR into vertically polarized radiation. The SR is focused on the AFM tip apex by a parabolic mirror [PM in Fig. 1].

The change in polarization direction is essential for s-SNOM operation, since a larger component of the electric field vector parallel to the tip axis increases the electric field enhancement at the tip apex. These fields interact locally with the surface of the sample by exciting a spectroscopic response. This is collected by the same near-field probe which acts as one arm of a Michelson interferometer. The second arm consists of a planar mirror which is mounted on a piezo stage and has been translated over a distance of 800 μm [I in Fig. 1]. The collected signal is recorded as an interferogram as a function of the optical beam path in the interferometer, which is subsequently Fourier transformed in order to derive an IR-spectrum. The spectral resolution of about 6 cm^{-1} is solely determined by the translation distance of the reference arm. A liquid-nitrogen cooled Mercury-Cadmium-Telluride (MCT) detector (J15D14, Teledyne Judson Technologies) [D in Fig. 1] with a sensitivity range from 2 μm to 13.5 μm was used for these experiments. For near-field imaging using a CO_2 gas laser we have used a pseudoheterodyne interferometric detection technique [51]. It is based on the

#252198 Received 19 Oct 2015; revised 17 Dec 2015; accepted 19 Dec 2015; published 13 Jan 2016

phase modulation of the reference wave and enables unambiguous imaging of the near-field optical amplitude and phase contrasts at a single laser line.

The investigated 1L-MoS_2 samples were grown in a tube furnace by chemical vapor deposition (CVD) onto a 300 nm thin SiO_2-layer on a Si substrate. Elemental sulfur and MoO_3 powder are used as S- and Mo-sources, respectively. The reactants were placed into alumina crucibles and inserted into a quartz tube, so that ultra-high purity nitrogen, used as a carrier gas, transports the sulfur vapor to the MoO_3 powder and onto the substrate, which is placed on top of the crucible containing MoO_3. The growth temperature was adjusted between 650 °C and 700°C [25, 52].

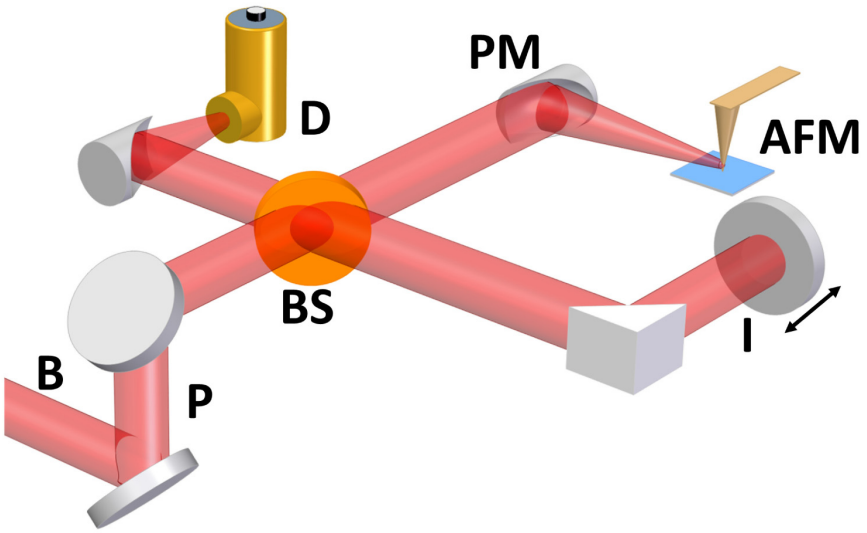

Fig. 1. Schematic diagram of the experimental setup. B represents the IR beam (SR or laser), P is a periscope-like mirror arrangement, BS denotes the ZnSe beam splitter, PM is a parabolic mirror, I corresponds to the translating mirror of the Michelson interferometer, D stands for the MCT detector, AFM is the atomic force microscope in the other arm of the interferometer.

3. Results and discussion

Figure 2(a) shows a 7 µm x 7 µm AFM topography image of a typical substrate area with MoS_2 triangular flakes. The edge length of the structures shown in the middle of Fig. 2(a) is approximately 6 µm.

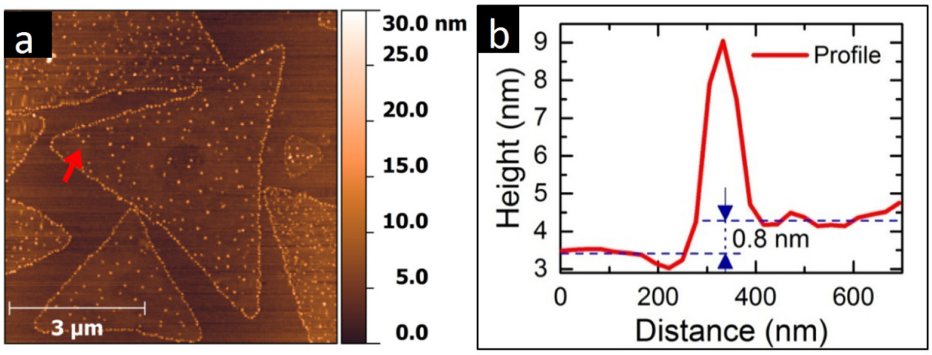

Fig. 2. MoS_2 monolayer structures on a SiO_2 substrate: (a) AFM topography image of various triangularly shaped MoS_2 flakes. The red arrow denotes the direction and the position of the cross section scan shown in (b); (b) line scan across the edge of a MoS_2 flake. The structure is approximately (0.8 ± 0.1) nm thick, which corresponds to a monolayer of MoS_2.

#252198 Received 19 Oct 2015; revised 17 Dec 2015; accepted 19 Dec 2015; published 13 Jan 2016

The height profile measured across the flake reveals a thickness of (0.8 ± 0.1) nm, representing a monolayer [cf. Figure 2(b)]. This result slightly differs from the expected theoretical thickness of 0.615 nm [53], which is commonly ascribed to a combination of different hygroscopicity/water accumulation on the SiO_2 substrate and the MoS_2 film as well as the AFM tapping mode, which has been reported to produce lower accuracy than in contact mode measurements, which has also been derived from the characterization of graphene samples [54]. The CVD MoS_2 islands contain occasionally bilayer growth seeds near their center. Compared to exfoliated layers CVD-grown samples exhibit stronger adhesion to the substrate [25]. Simultaneously to the topographic information, near-field intensity maps were acquired using a CO_2 laser source at 959.39 cm^{-1} (P2 line) [see Figs. 3(a)-3(e)]. An area of 7 µm x 7 µm in size was scanned at a resolution of 256 x 256 pixels and at an integration time of 20 ms per pixel. The first to the fifth harmonic signals were recorded (S_1-S_5), respectively. They denote the harmonics of the cantilever's oscillation frequency (Ω) at which the signal was demodulated. This is of crucial importance due to the relatively large size of the focused SR spot [47], which illuminates both tip and sample simultaneously. With the demodulation of the signal, and in combination with a lock-in amplifier, the strong far-field background can be separated from the weak near-field signal, where the latter is the signal of interest. Note that the demodulation works better when using higher harmonics (S_n, n>1). Higher harmonics signals correspond to decreasing the probing volume around the tip allowing for surface sensitive measurements [see Fig. 3(f)], as derived from ref [55].). The intensity maps of S_1-S_3 do not show a clear optical response of the 1L-MoS_2. The presence and definition of the 1L-MoS_2 can only be resolved by the increased contrast resulting from the side products of the MoS_2 growth process, such as MoO_3, which surround the triangular flakes and have an IR-absorption in the same spectral regime [56]. The signals recorded at higher harmonics (S_n, n > 3) reveal a difference in the near-field response between 1L-MoS_2 and SiO_2.

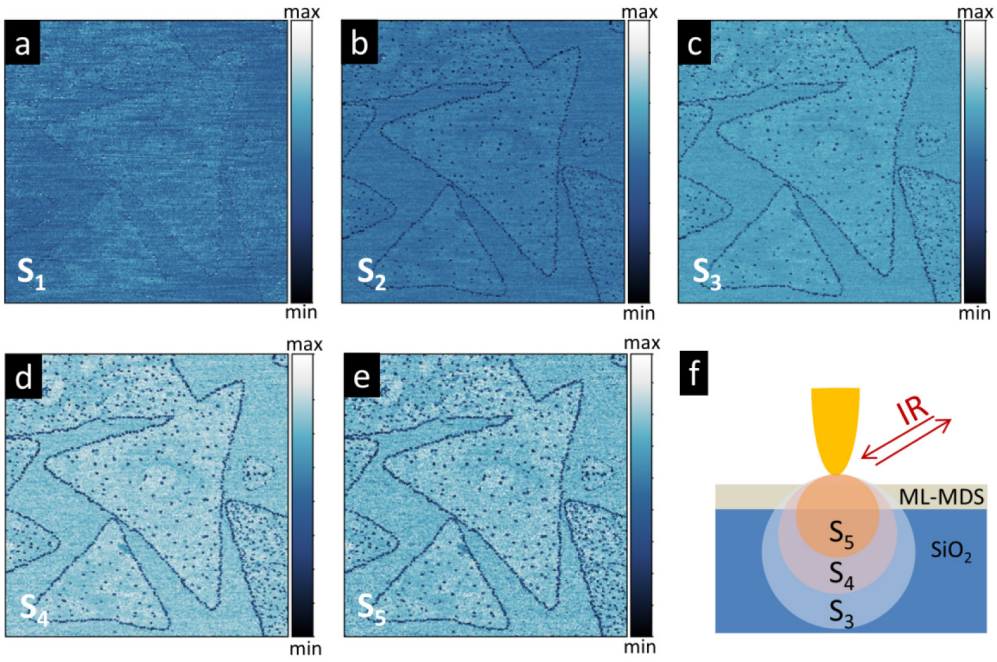

Fig. 3. The near-field intensity maps recorded at higher harmonics (S_n, $1 \le n \le 5$) of the tip's oscillation frequency using a CO_2 laser at 959.39 cm^{-1}: (a)-(e) illustrates the signals detected at S_1-S_5 respectively; (f) schematic presentation of the probed volume for different harmonics (reproduced according to [55]).

#252198 Received 19 Oct 2015; revised 17 Dec 2015; accepted 19 Dec 2015; published 13 Jan 2016

Here, the intensity of the former (the 1L-MoS_2) is higher. We attribute this difference in response to an enhancement of the SiO_2 layer near-field excitation in the presence of the local carrier concentration originating from the interaction of the 1L-MoS_2 with the tip. Mid IR radiation can excite collective charge oscillations in 1L-MoS_2 over a broad energy range [20] suggesting the presence of near-field enhancement over a wider frequency range than that of the SiO_2 phonon. The most significant advantage of using SR as a broadband IR radiation source is the ability to perform nano-FTIR spectroscopy over an energy range that is limited by the sensitivity range of the MCT detector only. Figure 4 presents near-field spectra derived from the 4th harmonic (S_4) recorded at the positions marked A and B on the 1L-MoS_2 structure and a third one labeled C on the SiO_2 substrate [inset of Fig. 4]. The reference mirror was translated over a distance of 800 μm at an integration time per data point of 100 ms. Each response is an average of two interferograms gathered successively at the same spatial position. The scattering amplitudes S_4 were normalized to (i) the near-field response of the Si reference-substrate using the same acquisition parameters and (ii) to the current of the storage ring. The 1L-MoS_2 double bond vibration around 469 cm^{-1} [57] could not be observed since the sensitivity range of the used MCT detector is limited to the spectral range from 740 to 5000 cm^{-1}. All spatially resolved spectra are dominated by an intense feature at ω_{SP1} = 1132 cm^{-1}. This is due to the surface phonon-polariton originating from the resonant near-field interaction between the SiO_2 and the probing tip. This finding is in agreement with results reported by other groups [39, 47, 58–61]. Additionally, the near-field signal gives rise to a less intense, lower-wavenumber response, ω_{SP2}, occurring around 794 cm^{-1}, which is due to a second surface phonon [39]. It occurs close to the transverse optical phonon frequency of SiO_2 (ω_{TO} = 797 cm^{-1}) [62].

The 1L-MoS_2 adlayer influences the near-field response of the SiO_2 substrate over a broad spectral range, as can be seen from the blue and red curves in Fig. 4(a) taken on the MoS_2 triangles as compared to the green curve on the bare substrate. Figure 4(a) reveals enhanced intensity of ω_{SP1} and ω_{SP2} on 1L-MoS_2 relative to bare SiO_2. This effect is evidently a result of the interaction of the surface phonons of the SiO_2 with the plasmons of 1L-MoS_2.

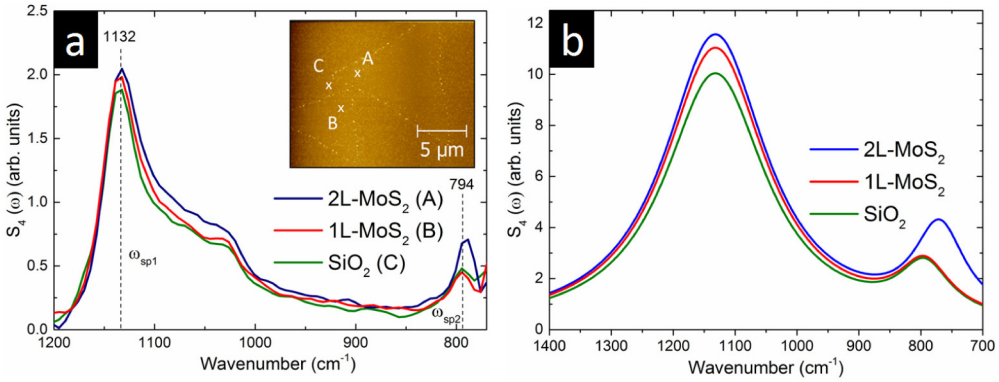

Fig. 4. (a) Nano-FTIR spectra of 1L-MoS_2 derived by Fourier transformation at the 4th harmonic of the interferograms recorded at the positions marked in the inset. The blue and red curves were acquired at positions A and B, respectively. They originate from 1L-MoS_2 that is deposited on 300 nm thick SiO_2. Position C corresponds to the bare SiO_2 substrate (green curve). Each spectrum represents the average of two interferograms gathered successively at the same positions; they were normalized to the Si response S_4 (1L-MoS_2 or SiO_2)/S_4(Si). ω_{SP1} and ω_{SP2} denote the frequencies of the SiO_2 phonon modes; (b) Theoretical results for the magnitude of the 4th s-SNOM scattering harmonics of SiO_2, 1L-MoS_2-SiO_2, and 2L-MoS_2-SiO_2 systems. It was assumed that the system's carrier concentration is 0.01 electron per MoS_2 unit cell (see text for further details).

#252198 Received 19 Oct 2015; revised 17 Dec 2015; accepted 19 Dec 2015; published 13 Jan 2016

In principle, the electron-phonon coupling is a macroscopic coupling of the electronic collective modes (plasmons) to the optical phonons that gives rise to the coupled plasmon-phonon modes, i.e. hybrid modes. This is similar to the graphene/SiO_2 interface which was intensely studied both teoretically [63] and experimentally [36, 39]. Contrary to those previous results, the 1L-MoS_2 plasmon coupling to the phonon modes does not exhibit a blueshift in the SiO_2 phonon relative to the bare substrate. To fully understand the underlying processes of phonon-plasmon interaction between 1L-MoS_2 and the SiO_2 substrate a deeper theoretical analysis is presented in the following Section.

4. Theoretical analysis

To calculate the s-SNOM intensity, we have used the point-dipole approximation for modeling the AFM-tip. This is valid in the case when the effective tip radius is much smaller than the characteristic wavelengths of the transition (see refs [36, 64].). To model the response of the coupled tip-sample system, we considered a tip with a radius a = 30 nm and polarizability a^3 that oscillates as $z_d(t) = b + z(t) = b + \Delta z(1-\cos(\Omega t))$, where $b = 0.7a$ is the initial distance between the tip and the surface. Δz = 40 nm, and Ω = 140-190 kHz are the tapping amplitude and frequency, respectively. The s-SNOM scattering harmonics of the demodulated signal, described by complex functions $s_n e^{i\varphi_n}$ (s_n is the amplitude and ϕ_n is the phase, n = 1, 2, 3, 4,…), were calculated as $s_n e^{i\varphi_n}$ =

$$\int_0^{2\pi} \frac{e^{in\phi} d\phi}{1 - G(b + \Delta z(1-\cos\phi), \omega) a^3}, \tag{1}$$

where the momentum-averaged sample-tip coupling function

$$G(z_d, \omega) = \int_0^{\infty} dq \cdot q^2 \cdot e^{-2qz_d} r_p(q, \omega), \tag{2}$$

depends on the distance between the oscillating tip and the surface b + Δz(1-cosϕ) [Eq. (1)] and on the frequency- and momentum-dependent reflection coefficient $r_p(q,\omega)$. The latter function, defined as the ratio of the amplitude of the P-polarized (transfer mode) reflected field to the amplitude of the P-polarized incident field, is the key quantity for modeling the s-SNOM spectrum. $r_p(q,\omega)$ fully describes the electrodynamics of the MoS_2-SiO_2 interface. It is calculated as:

$$r_p(q, \omega) = \frac{\varepsilon_1 k_0 - \varepsilon_0 k_1 + \frac{4\pi k_0 k_1 \sigma}{\omega}}{\varepsilon_1 k_0 + \varepsilon_0 k_1 + \frac{4\pi k_0 k_1 \sigma}{\omega}}, \tag{3}$$

where ε_0 and $\varepsilon_1 = \varepsilon_1(\omega,q)$ are the dielectric functions of vacuum and SiO_2, respectively. $\sigma = \sigma(\omega,q)$ denotes the in-plane conductivity of MoS_2. In Eq. (3), $k_{0,1} = (\varepsilon_{0,1}(\omega/c)^2 - q^2)^{1/2}$ are the out-of-plane components of the momenta, where q is the in-plane component of the momentum. To derive the expression for $r_p(q,\omega)$, we identified and took into account the following excitations that are relevant for the experimental results shown in Fig. 4. For SiO_2 these are the longitudinal and the transverse surface phonon modes at 1132 cm^{-1} and 794 cm^{-1}, respectively. Both [Fig. 4(b)] are clearly seen as peaks in the experimental SiO_2 nano-FTIR spectrum in Fig. 4(a). For MoS_2 islands the relevant excitations are plasmons. In a single layer island of MoS_2 [spot B, inset of Fig. 4(a)], the optical plasmon mode with the long wavelengths dispersion

#252198 Received 19 Oct 2015; revised 17 Dec 2015; accepted 19 Dec 2015; published 13 Jan 2016

$$\omega_{Pl}(q) = \omega_0 \sqrt{q(1 + \frac{3}{4}\frac{q}{q_{TF}})}, \quad (4)$$

contributes to the s-SNOM IR spectrum. In Eq. (4), $\omega_0 = (4e^2\varepsilon_F/(2\varepsilon_0))^{1/2}$ is the frequency, which is proportional to the bulk optical plasmon frequency. $q_{TF} = me^2/\varepsilon_0$ is the Thomas-Fermi momentum. Furthermore, e and m are the electron charge and mass, respectively. The Fermi energy $\varepsilon_F = \pi n/m$ is defined by the electron carrier density n and m (see, e.g., Ref [20]. for details). The plasmon spectrum of 2L-MoS_2 [spot A in Fig. 4] is modeled by

$$\omega_{Pl}(q) = \omega_{Pl}^{1L}(q)\sqrt{1 \pm e^{-|q|d}}, \quad (5)$$

where $\omega_{Pl}^{1L}(q) = \sqrt{\frac{2\pi e^2 n}{\varepsilon_0 m|q|}}$ is the 1L plasmon dispersion. Note that there is one extra mode compared to the 1L system [63, 65, 66]. The spectrum contains two modes: (i) the "standard" optical (+) mode, which is proportional to $\sqrt{|q|}$ at low momenta and (ii) a new acoustic (-) mode ($\sim|q|$), which corresponds to inter-plane oscillations. As we show below, the transverse low-energy mode plays a crucial role for the increase of the intensity of the 794 cm^{-1} peak in the experimental spectrum shown in Fig. 4(a).

Importantly, phonons in MoS_2 islands do not play an important role in the energy range presented in Fig. 4. In particular, our calculations on 1L-MoS_2 yield a phonon spectrum with energies below 500 cm^{-1}, which is in agreement with earlier experimental results [27, 67]. Furthermore, the phonon spectra of the 1L- and 2L-MoS_2 are rather similar in shape [57], as compared to the optical phonon energies. They are much lower than the energies of the SiO_2 modes that give rise to the intense spectral features shown in Fig. 4. Because of their different energies, one cannot expect strong hybridization between the MoS_2 and SiO_2 surface phonon modes and, hence, no significant shift of the s-SNOM spectra is anticipated. This resembles the case of graphene, where the relevant phonon modes have much higher energy than the SiO_2 modes (see, e.g., ref [68].) resulting in the absence of an observable spectral shift. For details of the derivation of the excitation spectra, dielectric functions, and $r_p(q,\omega)$, we refer to Ref [36]. The modeled spectra for the 4th harmonic of SiO_2, 1L-MoS_2-SiO_2, and 2L-MoS_2-SiO_2 systems are presented in Fig. 4(b).

The theoretical results, summarized in Fig. 4(b), are in agreement with the experimental data [see Fig. 4(a)]. It is important to note that the experimental results reveal that 1L-MoS_2-SiO_2, and 2L-MoS_2-SiO_2 systems do differ from the case of graphene [36]. Only for 2L-MoS_2 is a small spectral shift of ~5 cm^{-1} relative to the surface phonon peak of bare SiO_2 at 794 cm^{-1} seen. This redshift is due to the coupling of the silica phonon with the transverse 2L-MoS_2 plasmon mode. The fact that the corresponding coupling does not lead to a shift of the 1132 cm^{-1} peak in both 1L and 2L MoS_2 cases can be rationalized by the almost vertical orientation of the tip-sample electric field that leads to a preference for coupling predominantly to vertically oscillating modes.

Finally, we turn to the difference between the s-SNOM spectrum of MoS_2/SiO_2 and the corresponding spectrum for graphene. Contrary to our results, one observes a strong shift of the 1132 cm^{-1} peak of SiO_2 when it is coupled to graphene. Besides different momentum dependence, in graphene the plasmon dispersion is given by $\omega_{Pl}(q) = \omega_0\sqrt{q}(1 - \frac{q}{\bar{q}})$. More important is the difference of the dependence of the plasmon frequencies on the Fermi energy in these two systems. For graphene, the Fermi energy is proportional to the plasmon frequency and also to the square root of the carrier density n, $\varepsilon_F = (2\pi)^{1/2}\nu_F\sqrt{n}$, whereas for

#252198 Received 19 Oct 2015; revised 17 Dec 2015; accepted 19 Dec 2015; published 13 Jan 2016

MoS_2 it is proportional to the density of electrons, $\varepsilon_F = \pi n/m$, a much smaller number for a semiconductor with ~2 eV band gap. This leads to significantly lower plasmon frequencies in MoS_2, about 0.001 to 0.01 meV ($\sim n^{1/2}$), as compared to graphene ($\sim n^{1/4}$), where typical values of ~0.06 eV were found [36]. This is in agreement with the present experimental results. It is important to point out, that despite significantly lower plasmon frequencies as compared to graphene, one can still observe a notable shift of the ~800 cm^{-1} phonon mode in the case of 2L-MoS_2. Evidently, such shift is a resonance mode of the out-of-plane SiO_2 phonon and 2L-MoS_2 plasmon excitations, which is absent in graphene and 1L-MoS_2. Thus, we have demonstrated the capability of the s-SNOM technique to assign low-energy excitations in layered MoS_2 deposited on SiO_2 including substrate-MoS_2 interactions. Importantly, it is demonstrated that it is not required to have a Dirac-like spectrum to obtain a significant coupling between the substrate phonon- and 2D-material plasmon-modes. It cannot be fully excluded that some changes in the excitation spectra of 1L- and 2L-MoS_2 prepared by different techniques might occur, such as e.g. exfoliated MoS_2 samples, which can be rationalized due to possible defect states. However, we assume that such modifications of the system will not affect significantly the collective plasmon excitations, so that the results for the s-SNOM spectra shown in Fig. 4 will remain essentially unchanged.

5. Conclusion

We have demonstrated that SR-based near-field microscopy is a valuable tool not only for imaging monolayer thick MoS_2 structures deposited onto SiO_2 substrates, but also for investigating differences in the excitations in single and double layer islands of CVD-grown MoS_2. Our results revealed evidence of a strong interaction between the optical phonon modes of the SiO_2 and the plasmon modes of MoS_2 giving rise to hybrid plasmon-phonon modes. Depending on the number of layers, these modes exhibit an intensity enhancement as well as a spectral redshift compared to the SiO_2 phonon modes. The coupling strength between the surface modes strongly depends on the geometry of the system, i.e. the electric field distribution around the tip apex, which allows for an efficient excitation of the vertically oscillating modes. Our results are in agreement with theoretical calculations based on the point dipole model. The model calculations confirm that s-SNOM can be used to detect distinctly local excitations in layered systems, such as thickness variations, with high spatial resolution and surface sensitivity, providing the experimental and theoretical foundation to investigate other 2D-electronic materials.

Acknowledgments

Financial support by the German Research Foundation (DFG) within SFB 1112 (TP B02) is gratefully acknowledged. This work was supported by C-SPIN, part of STARnet, a Semiconductor Research Corporation program sponsored by MARCO and DARPA (SRC 2381.002 and 2381.003) and also supported partially by US DOE grant DE-FG02-07ER15842 and DE-FG02-07ER46354.

#252198 Received 19 Oct 2015; revised 17 Dec 2015; accepted 19 Dec 2015; published 13 Jan 2016